



Pham, X. N., Nguyen, M. B., & Doan, H. V. (2020). Direct synthesis of highly ordered Ti-containing Al-SBA-15 mesostructured catalysts from natural halloysite and its photocatalytic activity for oxidative desulfurization of dibenzothiophene. *Advanced Powder Technology*.  
<https://doi.org/10.1016/j.appt.2020.06.028>

Peer reviewed version

License (if available):  
CC BY-NC-ND

Link to published version (if available):  
[10.1016/j.appt.2020.06.028](https://doi.org/10.1016/j.appt.2020.06.028)

[Link to publication record in Explore Bristol Research](#)  
PDF-document

This is the author accepted manuscript (AAM). The final published version (version of record) is available online via Elsevier at <https://www.sciencedirect.com/science/article/pii/S092188312030306X> . Please refer to any applicable terms of use of the publisher.

## University of Bristol - Explore Bristol Research

### General rights

This document is made available in accordance with publisher policies. Please cite only the published version using the reference above. Full terms of use are available:  
<http://www.bristol.ac.uk/red/research-policy/pure/user-guides/ebr-terms/>

**Direct synthesis of highly ordered Ti-containing Al-SBA-15 mesostructured catalysts from natural halloysite and its photocatalytic activity for oxidative desulfurization of dibenzothiophene**

Xuan Nui Pham<sup>a,\*</sup>, Manh B Nguyen<sup>b</sup>, Huan V. Doan<sup>a,c</sup>

*<sup>a</sup>Department of Chemical Engineering, Hanoi University of Mining and Geology  
18 Vien Street, Bac Tu Liem District, Hanoi, Vietnam*

*<sup>b</sup>Institute of Research and Development, Duy Tan University, Da Nang 550000, Vietnam*

*<sup>c</sup>Department of Mechanical Engineering, University of Bristol, Bristol, BS8 1TH, UK*

\*Corresponding author: Assoc. Prof. Xuan Nui Pham

E-mail Address: [phamxuannui@gmail.com](mailto:phamxuannui@gmail.com) or [phamxuannui@humg.edu.vn](mailto:phamxuannui@humg.edu.vn)

**Abstract**

Here we show that bimetallic Ti-Al-SBA-15 materials were synthesized successfully from titanium tetraisopropoxide (TTIP) and natural halloysite clay via the direct hydrothermal method. The results revealed that the incorporation of titanium species in the Al-SBA-15 framework retained the characteristic peaks and possessed an increased Brunauer-Emmett-Teller (BET) surface area in comparison to the conventional Al-SBA-15 material. The successful isomorphous substitution of titanium in the Al-SBA-15 framework was confirmed by X-ray photoelectron spectroscopy (XPS) and Raman spectroscopies. The transmission electron microscopy (TEM) images showed that the composite material exhibited a highly ordered 2-D hexagonal mesostructure. The photocatalytic activity of these Ti-Al-SBA-15 mesoporous materials were assessed by dibenzothiophene (DBT) conversion under UV light irradiation, showing that the Al-SBA-15 sample containing 7.5 wt.% of titanium possessed the highest photocatalytic activity with a conversion of 92.68% at 70 °C and maintained the catalytic performance after four cycles. These

results suggest a promising technique to produce the Ti-Al-SBA-15 photocatalyst from an abundant and low-cost clay material.

*Keywords:* Halloysite, Ti-Al-SBA-15, titanium species, DBT, oxidative desulfurization.

## 1. Introduction

Doping titanium into molecular sieve materials, such as metallosilicates and zeolites, can provide enhanced performance of various photocatalytic reactions [1-5]. Accordingly, ordered mesoporous silica has attracted much attention as a catalyst support due to the discovery of porous inorganic solids of the 41S family by Mobil Research & Development Corporation [6]. Within the family of mesoporous materials, SBA-15 is a new mesoporous silica molecular sieve with tunable uniform hexagonal channels ranging from 5 nm to 30 nm. Its thick framework walls (3–5 nm) provide thermal stability that exceeds that of the thinner wall MCM-41 [7,8]. To date, the synthesis of mesoporous materials has been limited due to the need for expensive and toxic silica sources. To overcome these drawbacks, researchers have recently synthesized mesoporous materials using inexpensive inorganic silicate. Bentonite and kaolinite are natural widely available minerals. Bentonite mainly consists of montmorillonite, which is a 2:1 layered silicate and its unit layer structure consists of one  $\text{Al}^{3+}$  octahedral sheet placed between two  $\text{Si}^{4+}$  tetrahedral sheets, whereas kaolinite  $[\text{Al}_4(\text{Si}_4\text{O}_{10})(\text{OH})_8]$  is a 1:1 no swelling clay. Halloysite  $(\text{Al}_4[\text{Si}_4\text{O}_{10}](\text{OH})_8 \cdot 4\text{H}_2\text{O})$  is a dioctahedral 1:1 clay mineral of kaolin, in which an alumina of  $[\text{AlO}_6]$  octahedral sheet is related to a silica  $[\text{SiO}_4]$  tetrahedral sheet, consisting of hollow cylinders formed by multiple rolled layers [9,10]. Recently, Yang et al. [11] reported the synthesis of ordered mesoporous materials Al-MCM-41 from bentonite, with pretreated bentonite used as silica and aluminum sources. Fang et al. [2] synthesized titanium containing MCM-41 from industrial hexafluorosilicic acid as catalyst for epoxidation of cyclohexene. Shu et al. [12] proposed a novel template-free method for

1  
2  
3  
4 preparing mesoporous materials from natural minerals via the successive treatment of natural  
5  
6 kaolin by calcination, alkali activation and acid etching. Okada et al. [13,14] synthesized  
7  
8 mesoporous silicas and Al-containing mesoporous silicas by hydrothermal treatment of selectively  
9  
10 acid-treated saponite, acid leached metakaolinites. Kimura et al. [15] developed FSM-16-type  
11  
12 (p6mm) mesoporous silica via layered intermediates composed of fragmented silicate sheets.  
13  
14  
15

16  
17 The introduction of titanium species on the inner walls of SBA-15 can provide new  
18  
19 catalytic active sites due to the interaction of  $\text{TiO}_2$  with  $\text{SiO}_2$ . Ti-Al-SBA-15 material based on Al-  
20  
21 SBA-15 shows extraordinary thermal, hydrothermal, and hydrolytic stabilities, with the potential  
22  
23 as a photocatalyst [16–19]. However, the incorporation of titanium into the siliceous frameworks  
24  
25 of SBA-15 materials renders it difficult to create catalytic active sites under strongly acidic  
26  
27 conditions due to the hydrolysis of the Ti-O-Si network. To overcome the acidity, Xiao et al. [20]  
28  
29 prepared heteroatom substituted SBA-15 using the “pH-adjusting” method, while Li et al. [21]  
30  
31 prepared Ti-SBA-15 by controlling the hydrolysis of the siliceous source in the presence of  
32  
33 fluoride.  
34  
35  
36  
37  
38

39  
40 Titanium dioxide has also been incorporated into mesoporous silicalite-1 (TS-1) as a base  
41  
42 photocatalyst, with a sufficiently wide band gap to directly absorb visible light, exhibiting good  
43  
44 activity for the oxidation of bulky organics [22–24]. Khalid et al. [25] developed a single-pot  
45  
46 synthesis of NiMo-supported Ti-SBA-15 catalysts for hydrodesulfurization (HDS) of  
47  
48 dibenzothiophene. Andrea et al. [26] studied the oxidative desulfurization (ODS) of  
49  
50 dibenzothiophene in liquid fuel model with titanium-modified SBA-16, showing that the ODS  
51  
52 activities for nanometric  $\text{TiO}_2$  species of  $\text{TiO}_2/\text{SBA-16}$  sample achieved 90% of S removal at 60  
53  
54 °C in less than 1 h. Furthermore, Li et al. [27] studied a novel Ti-containing SBA-16-type  
55  
56  
57  
58  
59  
60  
61  
62  
63  
64  
65



mesoporous material directly synthesized by the evaporation-induced self-assembly method, showing that the photocatalyst was highly active in the oxidation of dibenzothiophene (DBT).

To the best of our knowledge, there is no report concerning the use of halloysite minerals for synthesis of Ti-Al-SBA-15 mesoporous structures. In this work, Ti-Al-SBA-15 was synthesized using the direct hydrothermal treatment method from natural halloysite without addition of silica and aluminum reagents. The physiochemical properties were investigated by X-ray diffraction (XRD), nitrogen adsorption-desorption measurements ( $N_2$  sorption), transmission electron microscopy (TEM), diffuse reflectance ultraviolet-visible spectroscopy (DR UV-vis), Fourier transform Raman spectroscopy (FT-Raman), X-ray photoelectron spectroscopy (XPS), and scanning electron microscopy-energy dispersive spectrophotometer (SEM-EDS). The catalytic performance of mesoporous Ti-containing Al-SBA-15 for ODS of DBT was also investigated.

## 2. Experimental

### 2.1 Materials

Halloysite clay obtained from Yenbai Province (Vietnam) was milled and sieved, followed by oven drying at 373 K for 24 h, and had the following chemical compositions (mass percentage): 32.26  $SiO_2$ ; 13.67  $Al_2O_3$ ; 4.38  $Fe_2O_3$ ; 0.39  $TiO_2$ ; 2.75  $CuO$ ; 1.25  $MgO$ ; 22.70  $Na_2O$ ; and 22.60 loss on ignition (LOI). Triblock copolymer Pluronic P123 ( $EO_{20}-PO_{70}-EO_{20}$ , MW = 5800) used as template, titanium isopropoxide ( $Ti[OCH(CH_3)_2]_4$ , TIPP 98%), acetic acid ( $CH_3COOH$ , 99.7%), ethanol ( $C_2H_5OH$ , 99.7%), dibenzothiophene ( $C_{12}H_8S$ , 99%), *n*-octane ( $C_8H_{18}$ , 99%), hydrogen peroxide ( $H_2O_2$ , 30%) were purchased from Sigma-Aldrich. Concentrated HCl and NaOH aqueous solutions were used as the acid and base sources, respectively. All reagents were analytical grade and were used without further purification.

## 2.2 Synthesis of Ti-Al-SBA-15 from halloysite

Ti-Al-SBA-15 materials were synthesized using the alkali-leached sample and titanium isopropoxide as precursor solutions. Halloysite was treated following the procedure of Yan et al. [28]. First, 10 g of halloysite was calcined at 700 °C for 2 h in air at a heating rate of 5 °C min<sup>-1</sup>, then 100 mL of 2 M NaOH solution was added, stirred and aged at 80 °C for 24 h. The solution was cooled to room temperature, the supernatant was then filtered, washed, dried at 80 °C overnight to form the alkali-leached sample and used silicon and aluminum as sources. Secondly, a titanium precursor solution was prepared by dissolving titanium isopropoxide in mixed solvents (ethanol and acetic acid) with a molar ratio at 1 Ti[OCH(CH<sub>3</sub>)<sub>2</sub>]<sub>4</sub> : 10 C<sub>2</sub>H<sub>5</sub>OH : 1 CH<sub>3</sub>COOH and stirred for 1 h at room temperature.

The titanium containing Al-SBA-15 was obtained by the one-step synthesis method. In a typical synthesis, 4 g of the structure directing agent, Pluronic 123, was dissolved in 120 mL of 2 M HCl solution under stirring for 3 h at 40 °C. Then, 5 g of the alkali-leached sample mixed with a calculated amount of titanium precursor solution (0.55, 0.825 and 1.1 mL of TIPP) was added slowly under vigorous stir at 40 °C for 24 h. The resultant mixture was then transferred into a Teflon-lined steel autoclave and aged at 100 °C for 48 h. After aging, the resultant solid product was filtered, washed with deionized water and dried at 80 °C in an oven, before being calcined at 550 °C for 5 h in air at a heating rate of 2 °C min<sup>-1</sup>. The prepared samples were denoted as 5Ti-Al-SBA-15, 7.5Ti-Al-SBA-15 and 10Ti-Al-SBA-15 corresponding to 5, 7.5 and 10 wt.% of titanium in the samples, respectively. For comparison, an Al-SBA-15 sample without titanium was also synthesized via the same procedure, without the addition of the titanium precursor solution.

### 2.3 Characterization of Ti-Al-SBA-15

XRD patterns were recorded on a D8 Advance-Brucker instrument using  $\text{CuK}\alpha$  radiation ( $\lambda = 0.1549$ ), with the specific surface area calculated by the Brunauer-Emmett-Teller (BET) method in the 0.05–0.30  $P/P_0$  range. The pore size distribution and their volumes were derived from the desorption branch of the  $\text{N}_2$  isotherms using the Barrett-Joyner-Halenda (BJH) method. The Raman spectra of samples were analyzed by a LabRAM HR800 spectroscopy (HORIBA). The sample powder was placed in a clean glass sample holder and the spectra was recorded in a range from  $200\text{ cm}^{-1}$  to  $1500\text{ cm}^{-1}$ . UV-vis spectra were measured using a UV-Visible spectrophotometer, JASCO V-670 scanning spectrophotometer equipped with an integrating sphere from 200 nm to 800 nm, with  $\text{BaSO}_4$  as a reference material. TEM measurements were performed with a JEOL JEM-1010 operated at an accelerating voltage of 200 kV. XPS spectra were recorded using KRATOS Axis 165 (Shimadzu, Japan) with  $\text{Mg K}\alpha$  radiation (1253.6 eV). Chemical analysis was performed by EDS of Varian Vista Ax Energy-dispersive X-ray spectroscope.

### 2.4. Photocatalytic activity

Photocatalytic activity was evaluated by measuring the conversion of DBT solution (containing 500 ppm sulfur) in *n*-octane in the presence of the catalyst under UV light irradiation. In the typical experiment, 0.05 g of Ti-Al-SBA-15 photocatalysts and 20 mL of DBT solution were added to a 250 mL three-neck round bottomed flask with a water condenser, and the mixture stirred for 60 min in the dark to attain adsorption and temperature equilibrium. Then, 0.5 mL of 30% aqueous of  $\text{H}_2\text{O}_2$  was dropped into the flask and the mixture exposed to UV (35 W) while stirring at different temperatures (30, 50 and 70 °C). The reaction solution samples were collected every 60 min for 360 min. The catalyst was separated from sample solutions by a filter and the remaining sulfur content (ppm) evaluated by Shimadzu HPLC Series 20A using Waters X-Bridge C18

Column (25 cm×4 mm×5 μm). The chromatographic parameters were as follows: acetonitrile/H<sub>2</sub>O ratio of 70/30 (v/v), UV detector wavelength set at 315 nm, the flow rate at 1.3 mL min<sup>-1</sup>, and volume injection of 10 μl. The DBT conversion was determined by the following equation:

$$C(\%) = (C_0 - C_t)/C_0$$

where,  $C_0$  is the DBT concentration (ppm) at time  $t = 0$ ; and  $C_t$  is the DBT concentration (ppm) at time  $t$ .

### 3. Results and Discussion

#### 3.1. XRD characterization

XRD patterns and SEM images of the natural halloysite are presented in Fig. 1. The XRD diagram of the natural halloysite clay in Fig. 1a shows the main peaks at  $2\theta$  values of about 12.1°, 20.1°, 24.5°, 35.0°, 38.6°, 54.5° and 62.5° corresponding to the primary diffraction of the (001), (100), (002), (110), (003), (210) and (300) planes of the halloysite with JCPDS Card No. 29-1487. In addition, a minor amount of quartz ( $2\theta = 26.7^\circ$ ) was also observed in the XRD diagram, which is in agreement with a previously published pattern for halloysite [29]. The uniform “stick”-like shape is clear in the SEM image of halloysite (inset Fig. 1b).

#### Fig. 1.

The XRD patterns of Al-SBA-15 and Ti-Al-SBA-15 obtained from halloysite are shown in Fig. 2. As shown in Fig. 2A, the small-angle XRD patterns of the samples showed a well-resolved two-dimensional (2D)-hexagonal lattice symmetry, exhibiting a prominent peak below 1° of  $2\theta$  corresponding to  $hkl = (100)$ , and two lesser peaks at 1.65° and 1.8° of  $2\theta$  corresponding to (110) and (200), respectively. However, the intensities of diffraction peaks at  $d_{100}$  decreased

with increased titanium content, indicating that more titanium incorporated into framework of silica-alumina structure of Al-SBA-15 material may result in damage to the pore structure.

As shown in Table 1,  $a_0$  unit-cell parameter of Ti-Al-SBA-15 samples increased with Ti content, that may be due to the ionic radius of titanium species ( $\text{Ti}^{4+} = 0.72 \text{ \AA}$ ) [30] being much larger than that of silica species ( $\text{Si}^{4+} = 0.41 \text{ \AA}$ ) [31], corresponding to higher bond length of Ti–O (0.179 nm) than Si–O (0.161 nm). This may result in some Ti atoms becoming incorporated into framework and replacing Si atoms, which causes some deformation of the parent Al-SBA-15 tetrahedral coordination structure [32-34].

The wide-angle XRD patterns of all the samples are shown in Fig. 2B. There were no clear characteristic peaks at higher angles, indicative of amorphous substances, except the 10Ti-Al-SBA-15 sample which exhibited a weak peak corresponding to the bulk  $\text{TiO}_2$  at  $2\theta = 25.2^\circ$ . This peak may be due to the extra-framework anatase phase. This result suggests that titanium species were incorporated into the mesoporous silica framework.

## Fig. 2.

### 3.2. Energy-dispersive X-ray spectroscopy (EDX)

The EDX results (Fig. 3) show the existence of Al, O and Si elements corresponding to Al-SBA-15 and Ti, Al, O, and Si elements in the ordered domains of 7.5Ti-Al-SBA-15, with no other impurities observed.

## Fig. 3.

### 3.3. $\text{N}_2$ adsorption-desorption isotherms

Fig. 4 shows the nitrogen adsorption-desorption isotherms at 77 K for Al-SBA-15 and Ti-Al-SBA-15 samples, which exhibited a type IV adsorption isotherm with  $\text{H}_1$  hysteresis loop in the

$P/P_0$  range of 0.6–1.0, indicating that all samples retained a mesoporous structure and characteristic of porous condensation within uniform pores of parent SBA-15 after incorporation of titanium species [35]. The textural properties of the samples are listed in Table 1. The BET surface area of all samples was estimated to be between 630.49 m<sup>2</sup> g<sup>-1</sup> and 742.30 m<sup>2</sup> g<sup>-1</sup>. The pore diameter was calculated from desorption curves of the BJH, with a pore size distribution between 8.1 nm and 8.7 nm, indicating a slight increase in pore size with increasing Ti content of 10 wt.%. The results show that the BET surface area and pore volume of Ti-Al-SBA-15 samples are greater than that of Al-SBA-15 and decrease with increasing Ti content, perhaps due to the formation of excess TiO<sub>2</sub> particles.

**Fig. 4.**

**Table 1.**

### 3.4. Raman spectroscopy

Raman spectra of Al-SBA-15 and **7.5Ti-Al-SBA-15** are shown in Fig. 5. For the pure Al-SBA-15 sample, the band at 494 cm<sup>-1</sup> is attributed to the asymmetric stretching vibration of the Si-O-Si bond and the symmetric stretching of Si-O-Si observed at 787 cm<sup>-1</sup>. The band at 967 cm<sup>-1</sup> could be assigned to the n(SiOH) vibration of surface silanol groups present in the framework defects of the mesoporous structure [36,37]. The **7.5Ti-Al-SBA-15** sample shows a strong intensity band at 1109 cm<sup>-1</sup>, which was assigned to the asymmetric stretching mode of the Ti-O-Si bonds. This band could be due to the resonance Raman effects of the titanium species framework in tetrahedral coordination environments [38]. Furthermore, the bands at 144, 197, 395, 517 and 638 cm<sup>-1</sup> corresponded to the Ti-O framework vibrations of TiO<sub>2</sub> anatase phase, which was not found in the Raman spectra, indicating that the Ti<sup>4+</sup> ion exists in the framework of the solid Al-SBA-15.

**Fig. 5.**

### 3.5. X-ray photoelectron spectroscopy (XPS)

Here we used XPS as a technique to investigate the chemical nature of the active species in the catalyst. Fig. 6a presents the Ti 2p region showing Ti  $p_{3/2}$ –Ti  $p_{1/2}$  doublets. The peak at 457.5 eV corresponded to Ti  $2p_{3/2}$  and the one at 463.2 eV to  $2p_{1/2}$ , that can be assigned to the presence of tetrahedral coordination of  $Ti^{4+}$  ions [39–41]. Furthermore, the framework incorporating  $Ti^{4+}$  was verified by the O 1s (Fig. 6b). The XPS spectrum of O 1s showed a peak assigned to Ti–O with corresponding binding energy of 533.92 eV [42,43]. These results confirmed that titanium species were inserted in the framework of Al-SBA-15 mesoporous material.

**Fig. 6.**

### 3.6. Transmission electron microscopy (TEM)

The TEM images of Al-SBA-15 and 7.5Ti-Al-SBA-15 are shown in Fig. 7, clearly demonstrating the regular arrangements of the hexagonal mesopores. The regularity of these mesopores was not affected after the incorporation of titanium ions. The TEM images also show that the materials are highly porous, with a pore diameter of about 8–10 nm. These results were in good agreement with the  $N_2$  adsorption-desorption analysis data.

**Fig. 7.**

### 3.7. UV-vis spectra

The UV-vis diffuse reflectance spectra (DRS) of Al-SBA-15 and Ti-containing Al-SBA-15 samples are presented in Fig. 8. The Al-SBA-15 material exhibited a small shoulder peak centered at 216 nm corresponding to the Al-O bond, which is due to the oxygen-to-metal charge-transfer transition of four-coordinated framework aluminum, characteristic of the alumina-silica structure of Al-SBA-15 [44].

#### Fig. 8.

All Ti-Al-SBA-15 spectra exhibited two broad bands centered at 220 and 313 nm, corresponding to the charge-transfer transitions of oxygen to tetrahedrally coordinated Ti ions [21,45]. The intensity of these bands increased with the increasing titanium content in the starting gels from 5% to 10% in Al-SBA-15.

The band gap of the samples was calculated using formula  $E_g = 1240/\lambda$ , in which  $E_g$  is the band gap energy, and  $\lambda$  is the wavelength of the absorption edge. The band gap decreased from 3.18 to 2.93 eV with increasing titanium content of 5% to 7.5%, respectively, and a slight increase in band gap with increasing Ti content of 10 wt.% ( $E_g = 2.99$  eV), indicating that a separate anatase-like phase was not formed in any structure of Ti-Al-SBA-15 sample even with the high titanium content [46].

### 3.8. Catalytic activity

To evaluate the potential use of Ti-Al-SBA-15 materials as ODS photocatalysts, DBT were chosen as model fuel with *n*-octane as solvent (containing 500 ppm DBT) and H<sub>2</sub>O<sub>2</sub> as oxidant. The photocatalytic activity of the catalysts was evaluated under UV light irradiation, at 30, 50, and 70 °C, with a reaction time of 360 min. The ODS results are presented in Figs. 9–11. Notably, all



1  
2  
3  
4 Ti-Al-SBA-15 catalysts exhibited ODS of DBT. However, almost no photocatalytic  
5  
6 degradation was observed in the Al-SBA-15, indicating that the Al-SBA-15 is not as  
7  
8 photocatalytically active as the other samples, and adsorption of DBT is a function of time  
9  
10 in the first step. After that, with the presence of H<sub>2</sub>O<sub>2</sub>, degradation of DBT over Al-SBA-15  
11  
12 catalyst was about 13.3%, 18.7%, and 24.5% at 30 °C, 50 °C, and 70 °C, respectively, within  
13  
14 360 min of reaction. This degradation might be due to the presence of weak acid sites on the  
15  
16 catalyst surface. Fig. 9 shows the DBT conversion as a function of reaction time at 30 °C, with a  
17  
18 rapid increase in the conversion rate after 240 min. At this time, the DBT conversion achieved  
19  
20 39.93% using 5Ti-Al-SBA-15 catalyst, 50.64% using 7.5Ti-Al-SBA-15 catalyst, and 45.85%  
21  
22 using 10Ti-Al-SBA-15 catalyst. After 360 min, 55.62% DBT was converted with 7.5Ti-Al-SBA-  
23  
24 15 catalyst. The photocatalytic activity of Ti-Al-SBA-15 catalysts for ODS of DBT at 50 °C is  
25  
26 presented in Fig. 10, showing that the DBT conversion reached 77.63% with 7.5Ti-Al-SBA-15  
27  
28 after 360 min. Fig. 11 presents the results of the ODS process at 70 °C, showing that after 360 min,  
29  
30 the conversion of DBT was a maximum of 92.68% using the 7.5Ti-Al-SBA-15 catalyst. These  
31  
32 results indicate that increasing Ti content from 5.0% to 7.5% leads to an increase in the DBT  
33  
34 conversion from 67.22% to 77.63% at 50 °C, and from 80.54% to 91.22% at 70 °C. However, by  
35  
36 increasing Ti content to 10 wt.%, the conversion of DBT decreased to 70.24% and 86.26% at 50  
37  
38 and 70 °C, respectively, which may be due to the lower band gap energy, as well as the BET  
39  
40 surface area and pore volume of 10Ti-Al-SBA-15 photocatalyst compared to the other  
41  
42 photocatalysts. The reason could be that the excess TiO<sub>2</sub> might form aggregates blocking the  
43  
44 transfer of electrons and holes in Ti-Al-SBA-15 photocatalyst and decreasing the  
45  
46 performance. These results were in agreement with our previous research [47]. It was clear that  
47  
48 the maximum DBT conversion occurred at 70 °C, as this high reaction temperature promoted the  
49  
50  
51  
52  
53  
54  
55  
56  
57  
58  
59  
60  
61  
62  
63  
64  
65

decomposition of  $\text{H}_2\text{O}_2$  oxidant, thus increased the generation of hydroxyl radicals ( $\cdot\text{OH}$ ) formed on the surface of the catalysts, leading to the ODS of DBT.

**Fig. 9.**

**Fig. 10.**

**Fig. 11.**

As shown in Fig. 12, with Al-SBA-15 catalyst, the degradation of DBT is 24.5% after 360 min irradiation, because the Al-SBA-15 catalyst had no photocatalytic activity. Furthermore, the photolysis of DBT without any photocatalyst is negligible as the DBT concentration is almost unchanged (5.9% degradation of DBT after 360 min irradiation).

**Fig. 12.**

The photocatalytic activity of titanium catalyst for the degradation of DBT was related to the oxidizing agents. In the presence of titano-alumino-silicate material, DBT is known to be converted to form dibenzothiophene sulfoxide and dibenzothiophene sulfone by radical reaction [48-50]. The first step consists of the reaction between the titanium in the catalyst with the lone pair of electrons of oxygen of hydrogen peroxide which forms a titanium-peroxo complex. The Ti-O-Si chemical bond is broken and Ti-OOH and Si-OH are formed. Ti-peroxide complex undergoes a nucleophilic attack by the sulfur of DBT to form sulfoxide. In the following step, dibenzothiophene sulfoxide undergoes further oxidation with another titanium-peroxo complex and forms dibenzothiophene sulfone. The proposed mechanism of oxidation of dibenzothiophene with Ti-Al-SBA-15 catalyst is shown in Fig. 13.

**Fig. 13.**

### 3.9. Recycling

The stability of the photocatalyst was evaluated by recycling 7.5Ti-Al-SBA-15 for photo-oxidation of DBT under UV light irradiation. The ODS of DBT was repeated four times using the following operating conditions: 0.05 g catalyst, 20 mL of model fuel, temperature of 70 °C and reaction time of 360 min. After each run, the catalyst after ODS of DBT was separated, recovered, and used for the next run. The DBT conversion after 360 min is presented in Fig. 14, showing that the ODS of DBT reduced by approximately 1.5% in the fourth cycle, that may be due to the catalyst mass loss in the cyclic experiments. Nonetheless, the synthesized Ti-Al-SBA-15 photocatalyst maintained its activity and stability for several cycles.

**Fig. 14.**

### 4. Conclusions

In this study, Ti-incorporated Al-SBA-15 materials with different Ti content were prepared by a direct hydrothermal procedure from halloysite clay and titanium tetraisopropoxide precursors. Highly ordered mesoporous Ti-Al-SBA-15 catalysts with a specific surface area of up to 742.3 m<sup>2</sup> g<sup>-1</sup> and pore volume of 1.32 cm<sup>3</sup> g<sup>-1</sup> were synthesized from halloysite clay via treatment of natural halloysite by calcination, alkali activation and leaching. The Ti-Al-SBA-15 samples revealed long range order and regular 2-D hexagonal mesostructure. Titanium was effectively incorporated into the framework structure of the Al-SBA-15 material, as confirmed by Raman and XPS analysis. Regarding photocatalytic activity, the 7.5Ti-Al-SBA-15 catalyst converted more than 90% of the DBT solution containing 500 ppm S at 70 °C in 360 min under UV light irradiation, maintaining its efficiency and stability through four cycles.

## Acknowledgements

The authors thank National Foundation for Science and Technology Development (NAFOSTED) of Vietnam for the financial support of this work under contact **No. 105.99-2018.301.**

## References

- [1] K. Zhou, X.-D. Xie, C.-T. Chang, Photocatalytic degradation of tetracycline by Ti-MCM-41 prepared at room temperature and biotoxicity of degradation products, *Appl. Surf. Sci.* 416 (2017) 248–258. <http://dx.doi.org/10.1016/j.apsusc.2017.04.174>.
- [2] T. Liu, F. Jin, X. Wang, Y. Fan, M. Yuan, Synthesis of titanium containing MCM-41 from industrial hexafluorosilicic acid as epoxidation catalyst, *Catal. Today* 297 (2017) 316–323. <http://dx.doi.org/10.1016/j.cattod.2017.03.011>.
- [3] C. Galacho, M.M.L. Ribeiro Carrott, P.J.M. Carrott, Structural and catalytic properties of Ti-MCM-41 synthesised at room temperature up to high Ti content, *Microporous Mesoporous Mater.* 100 (2007) 312–321. doi:10.1016/j.micromeso.2006.11.018.
- [4] W.-T. Qiao, G.-W. Zhou, X.-T. Zhang, T.-D. Li, Preparation and photocatalytic activity of highly ordered mesoporous TiO<sub>2</sub>-SBA-15, *Mater. Sci. Eng. C* 29 (2009) 1498–1502. doi:10.1016/j.msec.2008.12.010.
- [5] M. Fadhli, I. Khedher, J.M. Fraile, Modified Ti/MCM-41 catalysts for enantioselective epoxidation of styrene, *J. Mol. Cat. A-Chem.* 420 (2016) 282–289. <http://dx.doi.org/10.1016/j.molcata.2016.05.001>.
- [6] J.S. Beck, J.C. Vartuli, W.J. Roth, M.E. Leonowicz, C.T. Kresge, K.D. Schmitt, C.T.W. Chu, D.H. Olson, E.W. Sheppard, S.B. McCullen, J.B. Higgins, J.L. Schlenker, A new family of mesoporous molecular sieves prepared with liquid crystal templates, *J. Am. Chem. Soc.* 114 (1992) 10834–10843.

- [7] D.Y. Zhao, J.L. Feng, Q.S. Huo, N. Melosh, G.H. Fredrickson, B.F. Chmelka and G.D. Stucky, Triblock copolymer syntheses of mesoporous silica with periodic 50 to 300 angstrom pores, *Science* 548 (1998) 279.
- [8] J. Jarupatrakorn, T.D. Tilley, Silica-supported, single-site titanium catalysts for olefin epoxidation. A molecular precursor strategy for control of catalyst structure, *J. Am. Chem. Soc.* 124 (2002) 8380–8388. doi: 10.1021/ja0202208.
- [9] E. Joussein, S. Petit, J. Churchman, B. Theng, D. Righi, B. Delvaux, Halloysite clay minerals a review, *Clay Miner.* 40 (2005) 383–426. doi: <https://doi.org/10.1180/0009855054040180>.
- [10] L. Guimarães, A.N. Enyashin, G. Seifert, H.A. Duarte, Structural, electronic, and mechanical properties of single-walled halloysite nanotube model, *J. Phys. Chem. C* 114 (2010) 11358–11363. doi: 10.1021/jp100902e.
- [11] H. Yang, Y. Deng, C. Du, S. Jin, Novel synthesis of ordered mesoporous materials Al-MCM-41 from bentonite, *Appl. Clay Sci.* 47 (2010) 351–355. doi:10.1016/j.clay.2009.11.050.
- [12] T. Li, Z. Shu, J. Zhou, Y. Chen, D. Yu, X. Yuan, Y. Wang, Template-free synthesis of kaolin-based mesoporous silica with improved specific surface area by a novel approach, *Appl. Clay Sci.* 107 (2015) 182–187. <http://dx.doi.org/10.1016/j.clay.2015.01.022>.
- [13] K. Okada, H. Yoshizaki, Y. Kameshima, A. Nakajima, C.D. Madhusoodana, Synthesis and characterization of mesoporous silica from selectively acid-treated saponite as the precursors, *J Colloid Interface Sci.* 314 (1) 2007 176-83. doi: 10.1016/j.jcis.2007.05.036.

- [14] C.D. Madhusoodana, Y. Kameshima, A. Nakajima, K. Okada, T. Kogure, K. J. Mackenzie, Synthesis of high surface area Al-containing mesoporous silica from calcined and acid leached kaolinites as the precursors, *J. Colloid Interface Sci.* 297 (2006) 724-731. doi: 10.1016/j.jcis.2005.10.051.
- [15] T. Kimura, K. Kuroda, Ordered mesoporous silica derived from layered silicates, *Adv. Funct. Mater.* 19 (2009) 511–527. doi: 10.1002/adfm.200800647.
- [16] K. Song, J.Q. Guan, Z.Q. Wang, C. Xu, Q.B. Kan, Post-treatment of mesoporous material with high temperature for synthesis super-microporous materials with enhanced hydrothermal stability, *Appl. Surf. Sci.* 255 (2009) 5843-5846. <https://doi.org/10.1016/j.apsusc.2009.01.016>.
- [17] Z.A. Allothman, A.W. Apblett, Metal ion adsorption using polyamine-functionalized mesoporous materials prepared from bromopropyl-functionalized mesoporous silica, *J. Hazard. Mater.* 182 (2010) 581-590. doi: 10.1016/j.jhazmat.2010.06.072.
- [18] W. Chang, J. Shin, G. Chae, S.R. Jang, B.J. Ahn, Microwave-assisted Sonogashira cross-coupling reaction catalyzed by Pd-MCM-41 under solvent-free conditions, *J. Ind. Eng. Chem.* 19 (2013) 739-743. <https://doi.org/10.1016/j.jiec.2012.11.002>.
- [19] Y.H. Wu, Y.P. Jin, J.L. Cao, P. Yilihan, Y.J. Wen, J.X. Zhou, Optimizing adsorption of arsenic(III) by NH<sub>2</sub>-MCM-41 using response surface methodology, *J. Ind. Eng. Chem.* 20 (2014) 2792-2800. <https://doi.org/10.1016/j.jiec.2013.11.009>.
- [20] S. Wu, Y. Han, Y.-C. Zou, J.-W. Song, L. Zhao, Y. Di, S.-Z. Liu, F.-S. Xiao, Synthesis of heteroatom substituted SBA-15 by the “pH-Adjusting” method, *Chem. Mater.* 16 (2004) 486-492.

- [21] W.-H. Zhang, J. Lu, B. Han, M. Li, J. Xiu, P. Ying, C. Li, Direct synthesis and characterization of titanium-substituted mesoporous molecular sieve SBA-15, *Chem. Mater.* (14) 2002 3413-3421.
- [22] C. Jin, G. Li, X. Wang, Y. Wang, L. Zhao, D. Sun, A titanium containing micro/mesoporous composite and its catalytic performance in oxidative desulfurization, *Microporous Mesoporous Mater.* 111 (2008) 236–242.
- [23] Y. Fang, H. Hu, Mesoporous TS-1: Nanocasting synthesis with CMK-3 as template and its performance in catalytic oxidation of aromatic thiophene, *Catal. Commun.* 8 (2007) 817–820.
- [24] L.Y. Kong, G. Li, X.S. Wang, Oxidative desulfurization of organic sulfur in gasoline over Ag/TS-1, *Energy Fuel* 20 (2006) 896–902.
- [25] A. S. Ganiyu, K. Alhooshani, S.A. Ali, Single-pot synthesis of Ti-SBA-15-NiMo hydrodesulfurization catalysts: Role of calcination temperature on dispersion and activity, *Appl. Catal. B* 203 (2017) 428–441.
- [26] L.P. Rivoira, V.A. Vallés, B.C. Ledesma, M.V. Ponte, M.L. Martínez, O.A. Anunziata, A.R. Beltramone, Sulfur elimination by oxidative desulfurization with titanium-modified SBA-16, *Catal. Today* 271 (2016) 102–113.
- [27] A.T. Shah, B. Li, Z.E.A. Abdalla, Direct synthesis of Ti-containing SBA-16-type mesoporous material by the evaporation-induced self-assembly method and its catalytic performance for oxidative desulfurization, *J. Colloid Interface Sci.* 336 (2009) 707–711.
- [28] C. Zhou, T. Sun, Q. Gao, A. Alshameri, P. Zhu, H. Wang, X. Qiu, Y. Ma, C. Yan, Synthesis and characterization of ordered mesoporous aluminosilicate molecular sieve



- from natural halloysite, J. Taiwan Ins. Chem. E 45 (2014) 1073–1079.  
<http://dx.doi.org/10.1016/j.jtice.2013.09.030>.
- [29] G.W. Brindley, Order-disorder in the clay mineral structures. In crystal structures of clay minerals and their X-ray identification, Mineralogist Society: London, 1980; p 125.
- [30] D. Sun, T. Kiyobayashi, H.T. Takeshita, N. Kuriyama, C.M. Jensen, X-ray diffraction studies of titanium and zirconium doped NaAlH<sub>4</sub>: elucidation of doping induced structural changes and their relationship to enhanced hydrogen storage properties, J. Alloys Compd. 337 (2002) 1–2. doi: 10.1016/S0925-8388(01)01955-7.
- [31] B.H. Park, Y.-I. Kim, K.H. Kim, Effect of silicon addition on microstructure and mechanical property of titanium nitride film prepared by plasma-assisted chemical vapor deposition, Thin Solid Films 348 (1999) 210–214.
- [32] N.N. Opembe, E. Vunain, A.K. Mishra, K. Jalama, R. Meijboom, Thermal stability of Ti-MCM-41, J. Therm. Anal. Calorim. 117 (2014) 701–710.
- [33] H. Song, J. Wang, Z.D. Wang, H.L. Song, F. Li, Z.S. Jin, Effect of titanium content on dibenzothiophene HDS performance over Ni<sub>2</sub>P/Ti-MCM-41 catalyst, J. Catal. 311 (2014) 257–265.
- [34] M.D.B. Fontes, D.M.D. Melo, J.M.D. Barros, R.M. Braga, G. Rodrigues, Kinetic study of the catalytic pyrolysis of elephant grass using Ti-MCM-41, Mater. Res.-Ibero-Am. J. Mater. 17 (2014) 216–219.
- [35] S.J. Gregg, K.S.W. Sing, Adsorption, surface area and porosity, Academic press: London, 1982.

- [36] G. Xiong, C. Li, Q. Xin, Z. Feng, Direct spectroscopic evidence for vanadium species in V-MCM-41 molecular sieve characterized by UV resonance Raman spectroscopy, *Chem. Commun.* 8 (2000) 677 - 678.
- [37] A. Zecchina, S. Bordiga, C. Lamberti, G. Ricchiardi, C. Lamberti, G. Ricchiardi, D. Scarano, G. Petrini, G. Leofanti, M. Mantegazza, Structural characterization of Ti centres in Ti-silicalite and reaction mechanisms in cyclohexanone ammoximation, *Catal. Today* 32 (1996) 97-106.
- [38] C. Li, G. Xiong, Q. Xin, J.K. Liu, P.L. Ying, Z. Feng, J. Li, W.B. Yang, Y.Z. Wang, G.R. Wang, X.Y. Liu, M. Lin, X.Q. Wang, E.Z. Min, UV resonance Raman spectroscopic identification of titanium atoms in the framework of TS- 1 zeolite, *Angew. Chem., Int. Ed.* 38 (1999) 2220 – 2222.
- [39] C. Yu, H. Chu, Y. Wan, D. Zhao, Synthesis of easily shaped ordered mesoporous titanium-containing silica, *J. Mater. Chem.* 20 (2010) 4705–4714. doi: 10.1039/b925864g.
- [40] J.F. Moulder, *Handbook of X-ray photoelectron spectroscopy: A reference book of standard spectra for identification and interpretation of XPS data*, Physical electronics division, Perkin-Elmer Corporation, 1992.
- [41] T.A. Zepeda, Comparison and performance of different sulphided Ti-loaded mesostructured silica-supported CoMo catalysts in deep HDS, *Appl. Catal. A-Gen.* 347 (2008) 148–161. doi:10.1016/j.apcata.2008.06.012.
- [42] R.S. Araújo, D.C.S. Azevedo, E. Rodríguez-Castellón, A. Jiménez-López, C.L.Jr. Cavalcante, Al and Ti-containing mesoporous molecular sieves: Synthesis,

- characterization and redox activity in the anthracene oxidation, *J. Mol. Catal. A- Chem.* 281 (2008) 154–163. doi:10.1016/j.molcata.2007.09.001.
- [43] Z. Luan, E.M. Maes, P.A.W. van der Heide, D. Zhao, R.S. Czernuszewicz, L. Kevan, Incorporation of titanium into mesoporous silica molecular sieve SBA-15, *Chem. Mater.* 11 (1999) 3680-3686. doi:org/10.1021/cm9905141.
- [44] F. Akti, Effect of kaolin on aluminum loading success in synthesis of Al-SBA-15 catalysts: Activity test in ethanol dehydration reaction, *Micropor. Mesopor. Mat.* 294 (2020) 109894. doi.org/10.1016/j.micromeso.2019.109894.
- [45] W. Zhan, J. Yao, Z. Xiao, Y. Guo, Y. Wang, Y. Guo, G. Lu, Catalytic performance of Ti-SBA-15 prepared by chemical vapor deposition for propylene epoxidation: The effects of SBA-15 support and silylation, *Micropor. Mesopor. Mat.* 183 (2014) 150–155.
- [46] C. Galacho, M.M.L. Ribeiro Carrott, P.J.M. Carrott, Structural and catalytic properties of Ti-MCM-41 synthesised at room temperature up to high Ti content, *Micropor. Mesopor. Mat.* 100 (2007) 312–321.
- [47] X.N. Pham, B.M. Nguyen, H.T. Thi, H.V. Doan, Synthesis of Ag-AgBr/Al-MCM-41 nanocomposite and its application in photocatalytic oxidative desulfurization of dibenzothiophene, *Adv. Powder Technol.* 29 (2018) 1827–1837. <https://doi.org/10.1016/j.appt.2018.04.019>.
- [48] X.N. Pham, D.L. Tran, T.D. Pham, Q.M. Nguyen, V.T.T. Thi, H.D. Van, One-step synthesis, characterization and oxidative desulfurization of 12-tungstophosphoric

heteropolyanions immobilized on amino functionalized SBA-15, Adv. Powder Technol. 29 (2018) 58–65.

- [49] X.N. Pham, T.D. Pham, B.M. Nguyen, H.T. Tran, D.T. Pham, Synthesis of Al-MCM-41@Ag/TiO<sub>2</sub> nanocomposite and its photocatalytic activity for degradation of dibenzothiophene, J. Chem. 2018 ID 8418605, 9 pages.
- [50] B. Saha, S. Kumar, S. Sengupta, Green synthesis of nano silver on TiO<sub>2</sub> catalyst for application in oxidation of thiophene, Chem. Eng. Sci. 199 (2019) 332–341.

**Figures caption**

**Fig. 1.** (a) XRD patterns, (b) SEM image and powder sample (inset) of natural halloysite.

**Fig. 2.** (A) Small-angle and (B) wide-angle of XRD patterns of (a) the synthesized Al-SBA-15(b) 5Ti-Al-SBA-15, (c) 7.5Ti-Al-SBA-15 and (d) 10Ti-Al-SBA-15 from halloysite.

**Fig. 3.** EDX analysis of (a, b) Al-SBA-15 and (b) 7.5Ti-Al-SBA-15.

**Fig. 4.** (A) Nitrogen adsorption-desorption isotherms and (B) pore size distribution of (a) Al-SBA-15, (b) 5Ti-Al-SBA-15, (c) 7.5Ti-Al-SBA-15 and (d) 10Ti-Al-SBA-15 samples.

**Fig. 5.** Raman spectra of (a) Al-SBA-15 and (b) 7.5Ti-Al-SBA-15 photocatalysts.

**Fig. 6.** XPS spectrum of 7.5Ti-Al-SBA-15: (a) Ti 2p spectrum and (b) O 1s spectrum.

**Fig. 7.** TEM images of (a, b) Al-SBA-15 and (c, d) 7.5Ti-Al-SBA-15 materials.

**Fig. 8.** The UV-vis DRS of (a) Al-SBA-15 and (b) 5Ti-Al-SBA-15, 7.5Ti-Al-SBA-15, 10Ti-Al-SBA-15 photocatalysts.

**Fig. 9.** Conversion of DBT as a function of reaction time at 30 °C. Conditions: 20 mL model fuel; 0.05 g catalyst; 0.5 mL H<sub>2</sub>O<sub>2</sub>.

**Fig. 10.** Conversion of DBT as a function of reaction time at 50 °C. Conditions: 20 mL model fuel; 0.05 g catalyst; 0.5 mL H<sub>2</sub>O<sub>2</sub>.

**Fig. 11.** Conversion of DBT as a function of reaction time at 70 °C. Conditions: 20 mL model fuel; 0.05 g catalyst; 0.5 mL H<sub>2</sub>O<sub>2</sub>.

**Fig. 12.** Conversion of DBT as a function of reaction time at 70 °C. Conditions: 20 mL model fuel; with 0.05 g catalyst and without catalyst; 0.5 mL H<sub>2</sub>O<sub>2</sub>.

**Fig. 13.** Proposed mechanism for the oxidation of dibenzothiophene with Ti-Al-SBA-15 catalyst.

**Fig. 14.** Recycling activity of 7.5Ti-Al-SBA-15 photocatalyst for ODS of DBT. Conditions: 20 mL model fuel; 0.05 g catalyst; 0.5 mL H<sub>2</sub>O<sub>2</sub>; reaction temperature 70 °C.

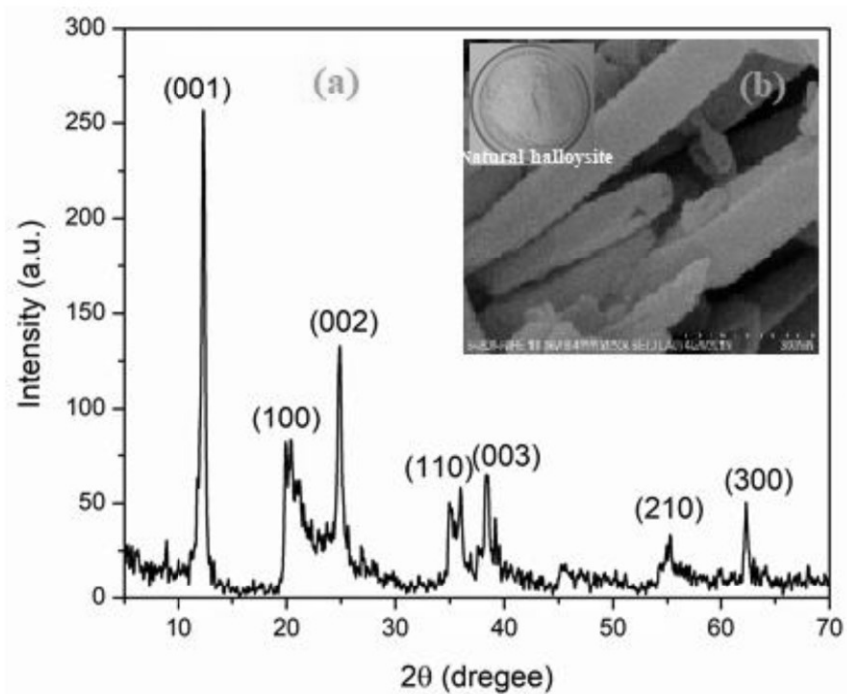


**Fig. 1.** (a) XRD patterns, (b) SEM image and powder sample (inset) of natural halloysite.

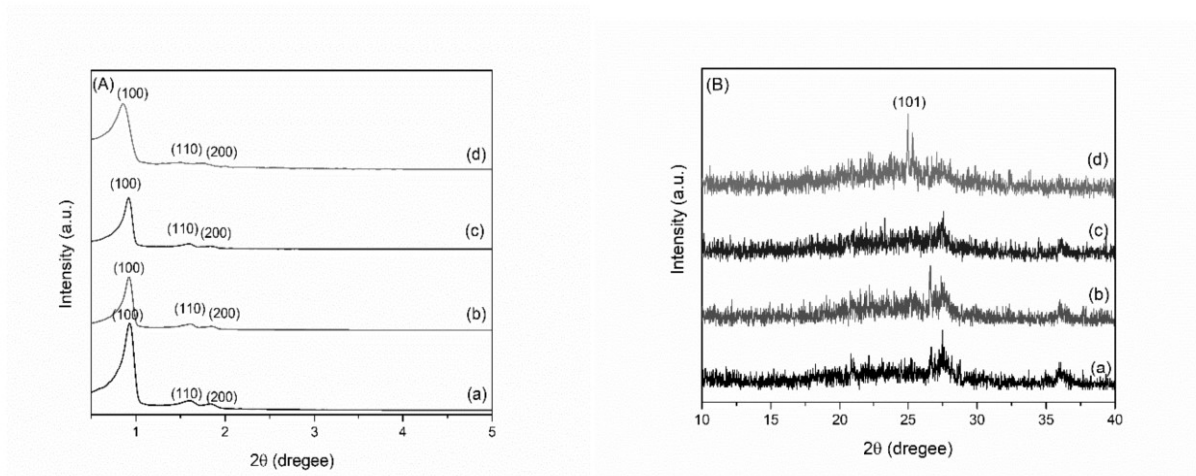


**Fig. 2.** (A) Small-angle and (B) wide-angle of XRD patterns of (a) the synthesized Al-SBA-15 (b) 5Ti-Al-SBA-15, (c) 7.5Ti-Al-SBA-15 and (d) 10Ti-Al-SBA-15 from halloysite.



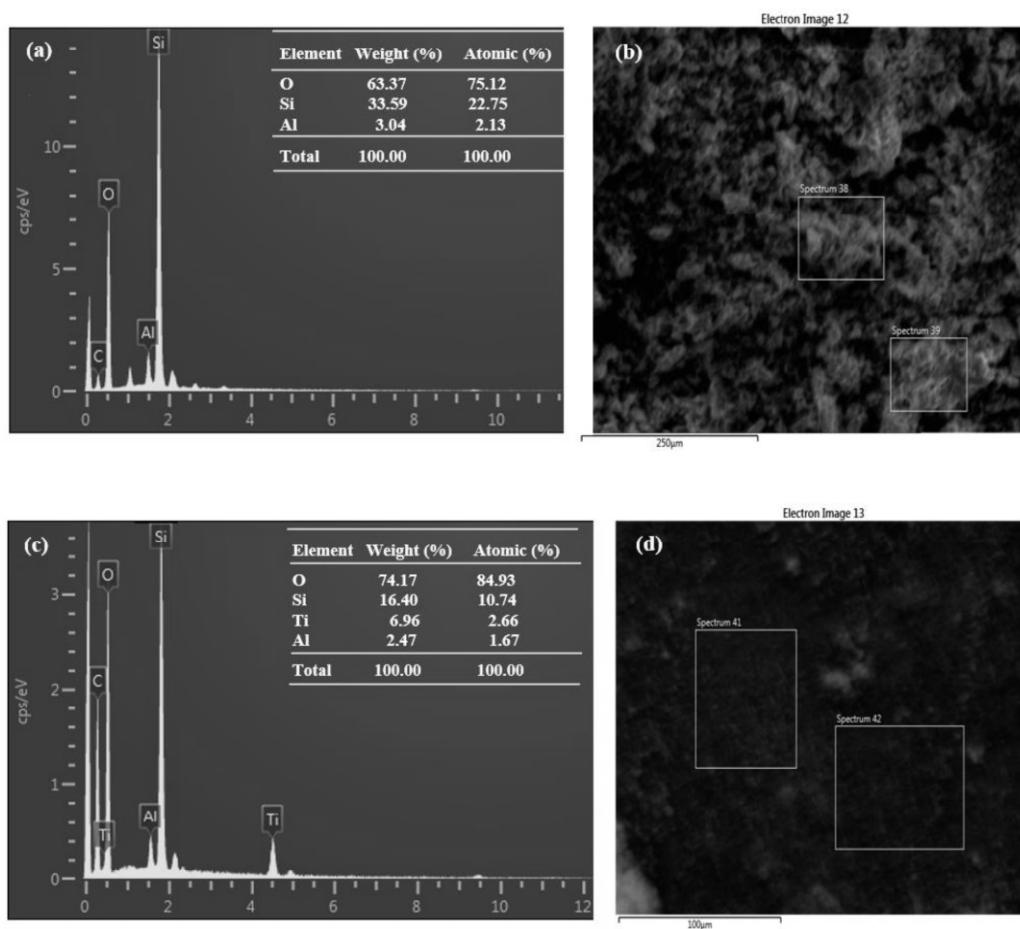


**Fig. 3.** EDX analysis of (a, b) Al-SBA-15 and (b) 7.5Ti-Al-SBA-15.

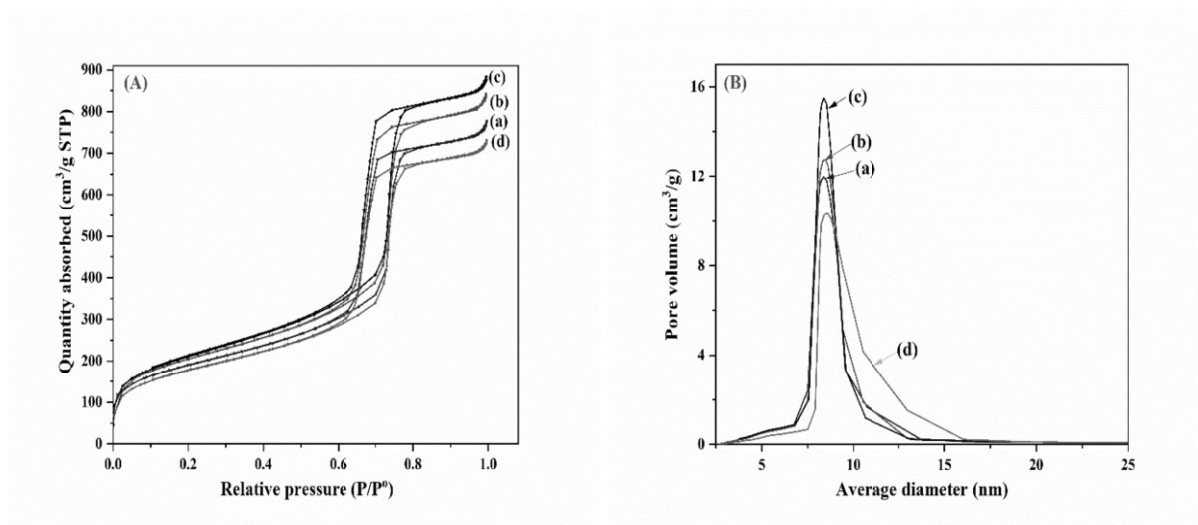


**Fig. 4.** (A) Nitrogen adsorption-desorption isotherms and (B) pore size distribution of (a) Al-SBA-15, (b) 5Ti-Al-SBA-15, (c) 7.5Ti-Al-SBA-15 and (d) 10Ti-Al-SBA-15 samples.

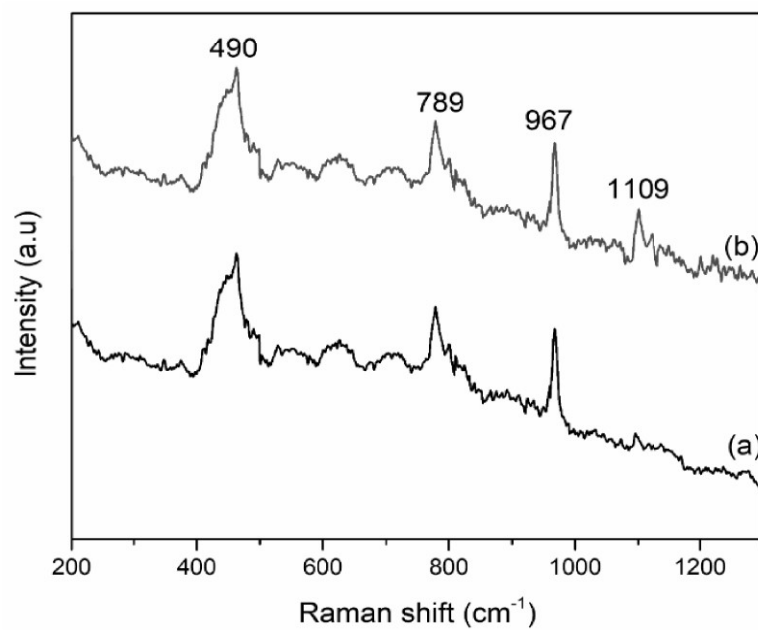


**Fig. 5.** Raman spectra of (a) Al-SBA-15 and (b) 7.5Ti-Al-SBA-15 photocatalysts.

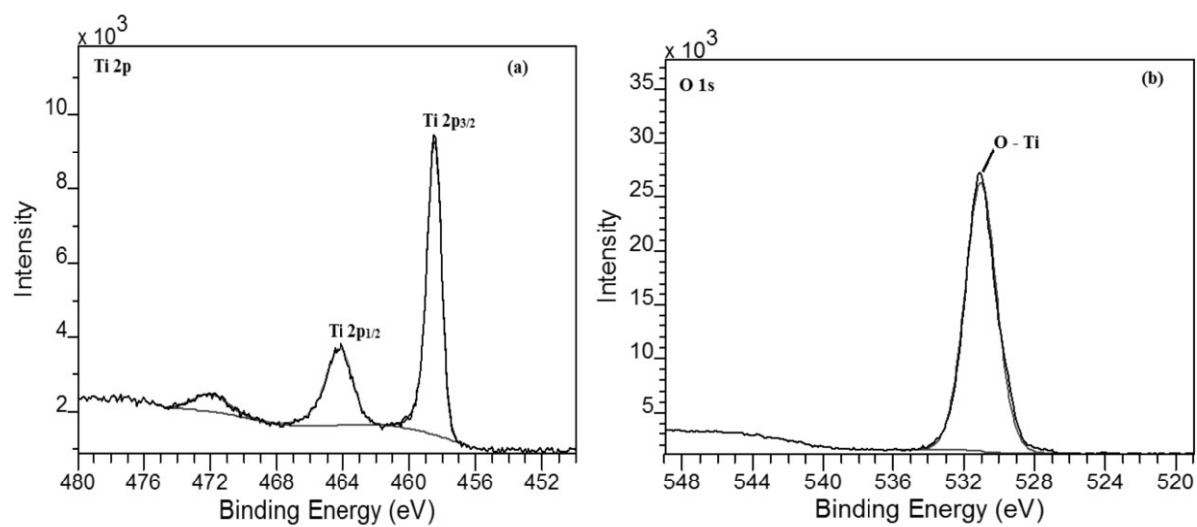


**Fig. 6.** XPS spectrum of 7.5Ti-Al-SBA-15: (a) Ti 2p spectrum and (b) O 1s spectrum.

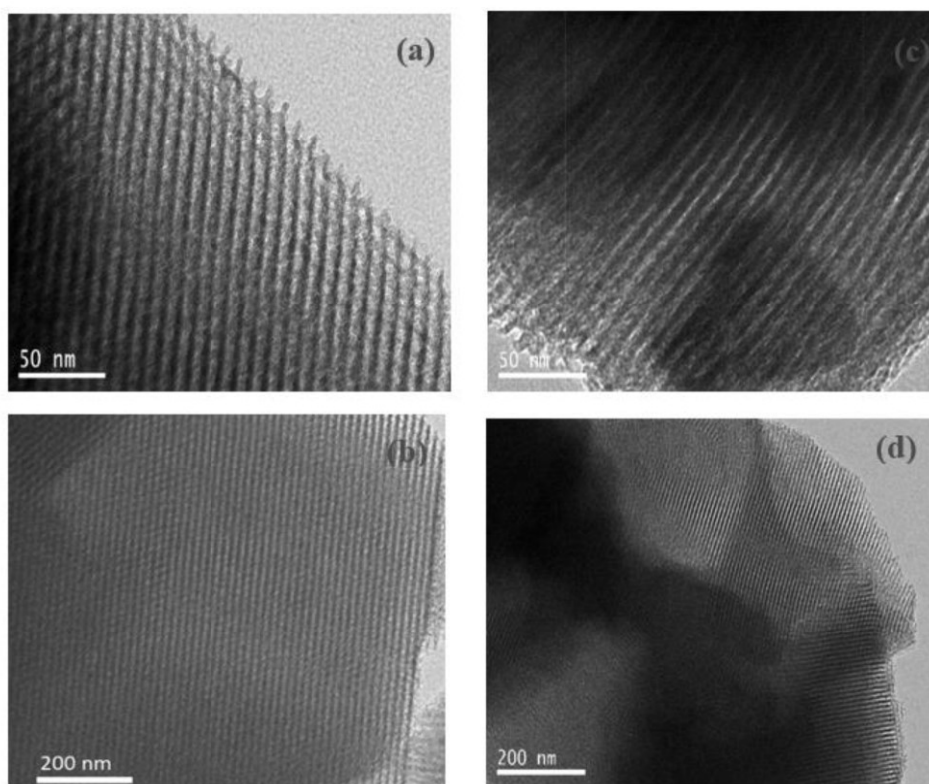


**Fig. 7.** TEM images of (a, b) Al-SBA-15 and (c, d) 7.5Ti-Al-SBA-15 materials.

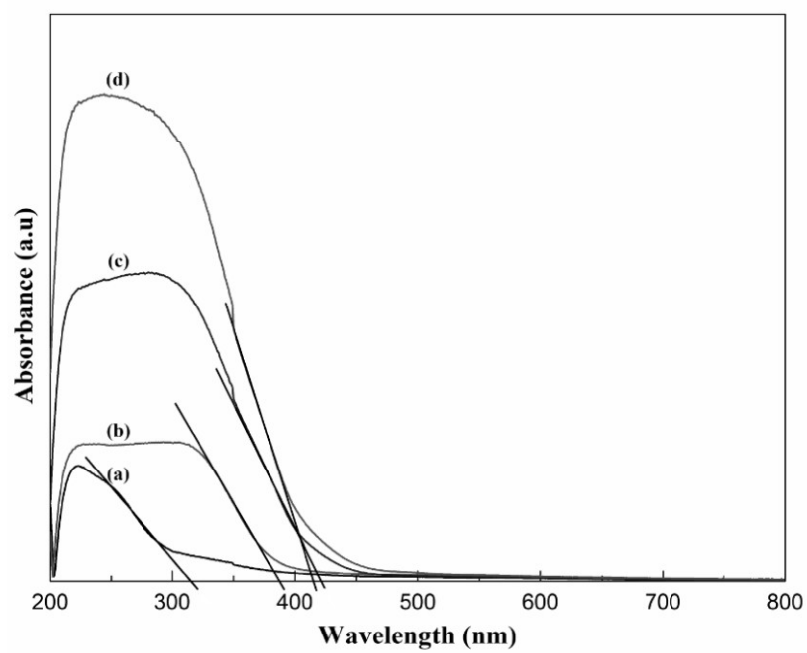


**Fig. 8.** The UV-vis DRS of (a) Al-SBA-15, (b) 5Ti-Al-SBA-15, (c) 7.5Ti-Al-SBA-15 and (d) 10Ti-Al-SBA-15 photocatalysts.

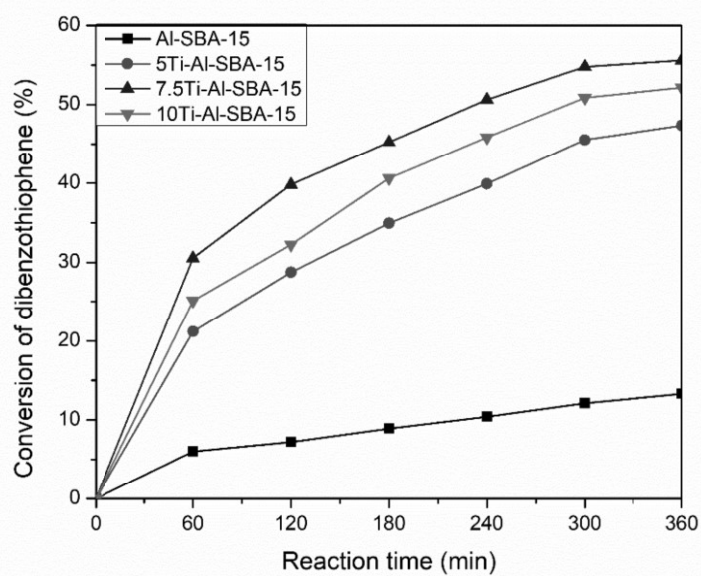


**Fig. 9.** Conversion of DBT as a function of reaction time at 30 °C. Conditions: 20 mL model fuel; 0.05 g catalyst; 0.5 mL H<sub>2</sub>O<sub>2</sub>.

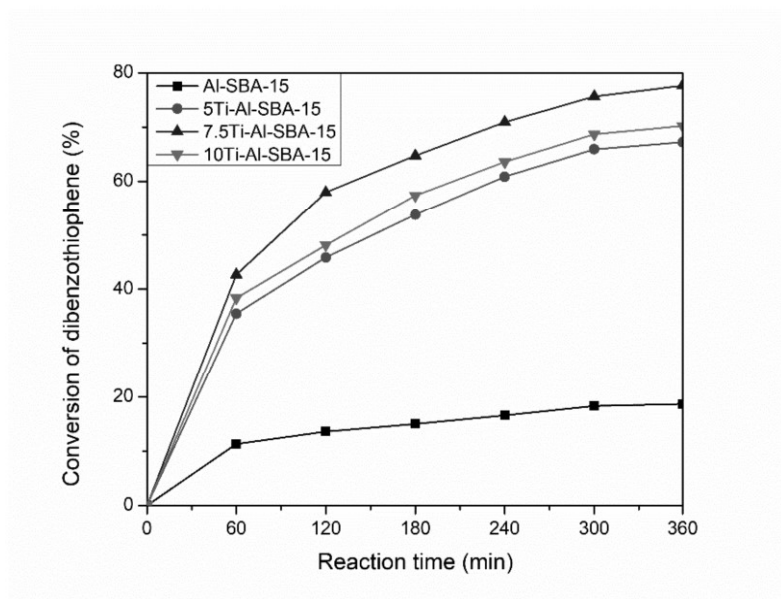


**Fig. 10.** Conversion of DBT as a function of reaction time at 50 °C. Conditions: 20 mL model fuel; 0.05 g catalyst; 0.5 mL H<sub>2</sub>O<sub>2</sub>.



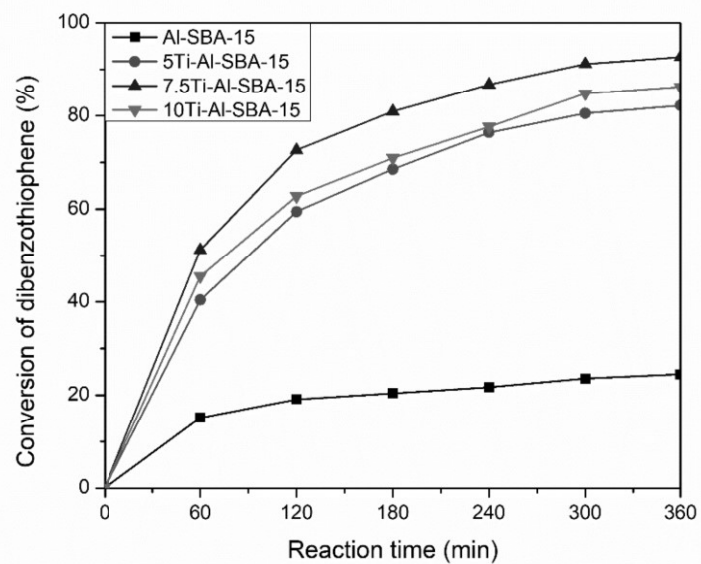


**Fig. 11.** Conversion of DBT as a function of reaction time at 70 °C. Conditions: 20 mL model fuel; 0.05 g catalyst; 0.5 mL H<sub>2</sub>O<sub>2</sub>.

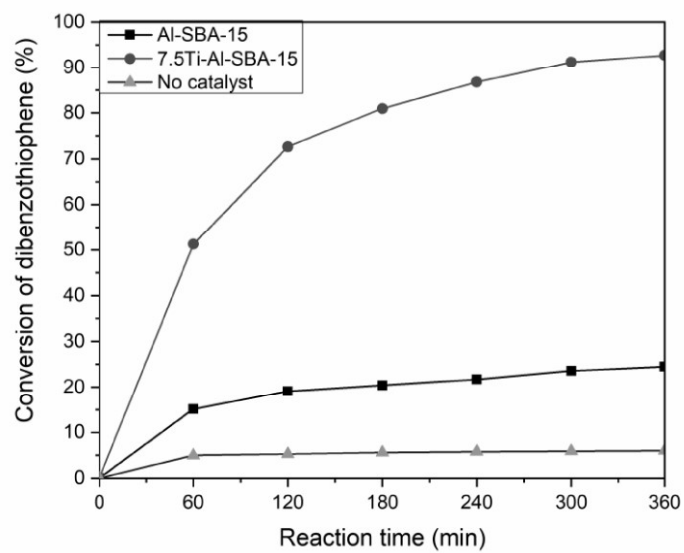


**Fig. 12.** Conversion of DBT as a function of reaction time at 70 °C. Conditions: 20 mL model fuel; with 0.05 g catalyst and without catalyst; 0.5 mL H<sub>2</sub>O<sub>2</sub>.

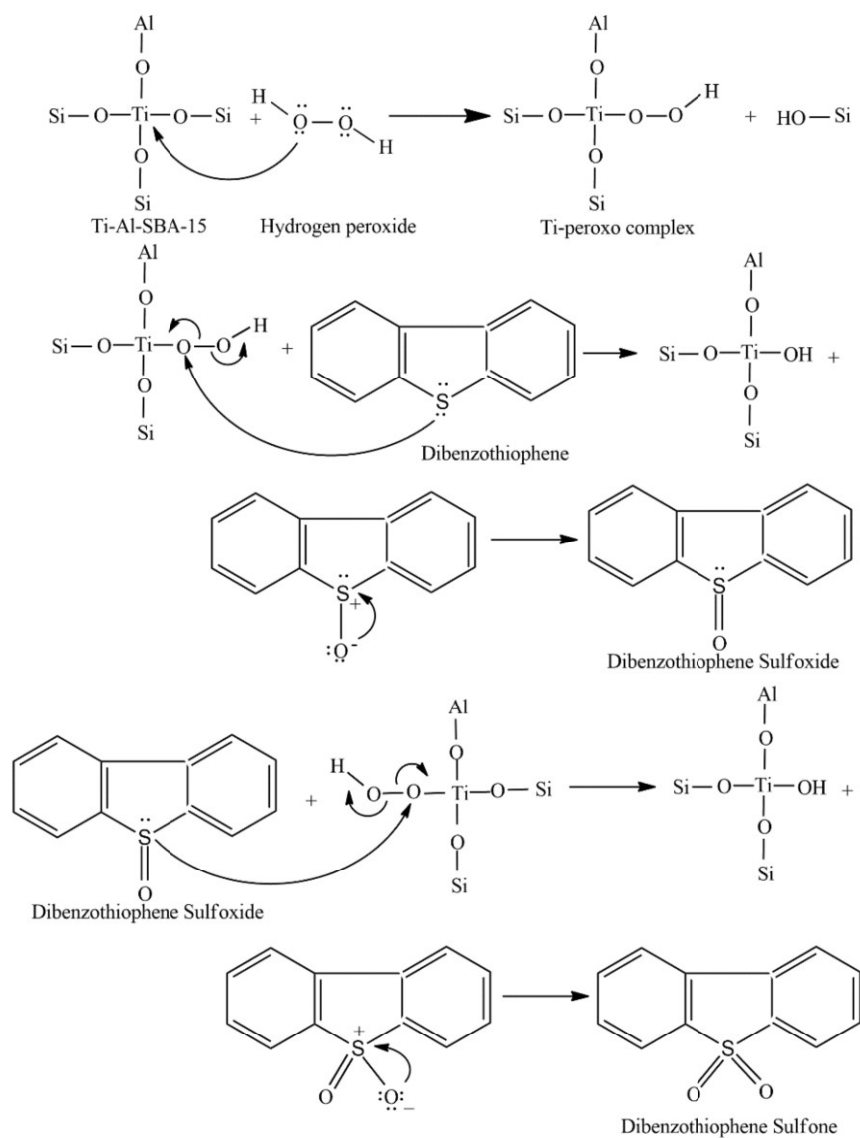


**Fig. 13.** Proposed mechanism for the oxidation of dibenzothiophene with Ti-Al-SBA-15 catalyst

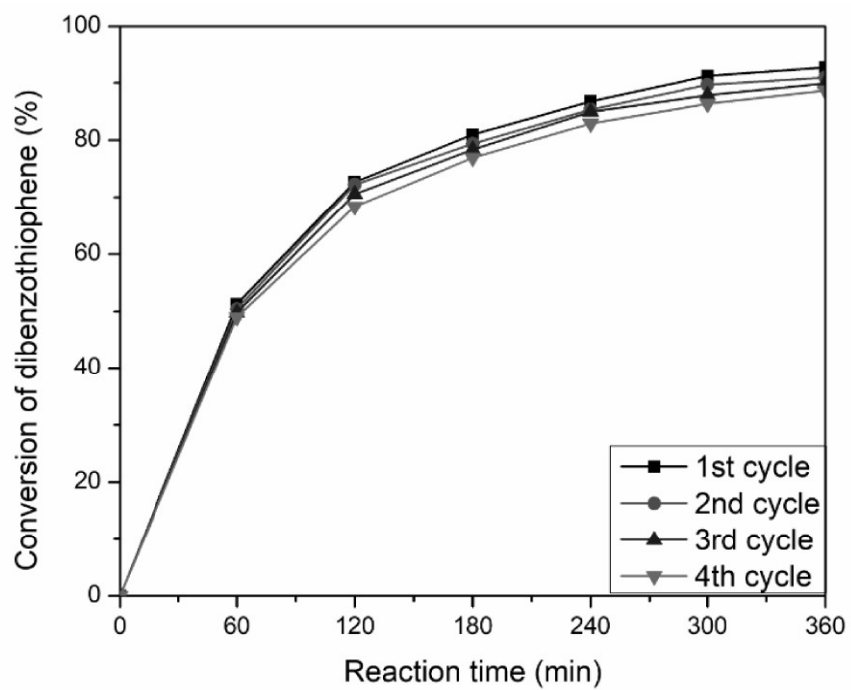


**Fig. 14.** Recycling activity of 7.5Ti-Al-SBA-15 photocatalyst for ODS of DBT. Conditions: 20 mL model fuel; 0.05 g catalyst; 0.5 mL H<sub>2</sub>O<sub>2</sub>; reaction temperature 70 °C.